Available online at www.sciencedirect.com
ScienceDirect
Scripta Materialia 59 (2008) 1159–1162
Scripta MATERIALIA
www.elsevier.com/locate/scriptamat

Aluminum-rich bulk metallic glasses

B.A. Sun,[a] M.X. Pan,[a] D.Q. Zhao,[a] W.H. Wang,[a,*] X.K. Xi,[b] M.T. Sandor[b] and Y. Wu[b]

[a] *Institute of Physics, Chinese Academy of Sciences, Beijing 100190, China*
[b] *Department of Physics and Astronomy, University of North Carolina, Chapel Hill, NC 27599-3255, USA*

Received 14 July 2008; revised 31 July 2008; accepted 2 August 2008
Available online 14 August 2008

The formation and properties of a class of Al-rich bulk metallic glasses (BMGs) are reported. The Al contents for these alloys can reach up to 40 at.%, which is the highest in known BMGs. The Al-rich BMGs deviate greatly from eutectic composition and show high thermal stability and fragility, and very high mechanical strength. These Al-rich BMGs might have implications for Al-based BMGs in general and for understanding the role of Al in glass formation.

Keywords: Metallic glasses; Casting

Bulk metallic glasses (BMGs) have attracted a great deal of interest because of their extraordinary properties and their potential for practical applications [1]. A large number of BMGs based on different elements such as Zr, Fe, Cu, rare earth (RE) and Mg have been obtained recently [1–6]. Compared to other alloy systems, Al-based metallic glass is of particular interest because of its low density and potential aerospace applications [7]. However, Al-based metallic glasses are very different from conventional BMG-forming systems. One of main differences is that the glass formation range in Al-based metallic glasses lies on the solute-rich side of the eutectic point where the liquidus temperature rises steeply, resulting in a greatly reduced glass transition temperature $T_{rg} = T_g/T_l$, normally less than 0.5 [8]. Furthermore, the glass-forming ability (GFA) of Al-based metallic glasses does not follow the atomic size criteria employed for producing BMGs [9]. To date, Al-based BMGs thicker than 1 mm have not yet been produced. On the other hand, Al is an indispensable additive for improving the GFA and other properties in many BMG-forming alloys [1,2]. For example, the critical thickness of Nd–Fe amorphous alloys is usually less than 30 μm, and addition of Al can drastically improve the GFA in this alloy, resulting in the formation of Nd–Fe–Al BMGs with a thickness exceeding 10 mm and good hard magnetic properties [10]. Furthermore, addition of 5% Al greatly increases the GFA of binary $Cu_{50}Zr_{50}$ alloy and the resulting $Cu_{47.5}Zr_{47.5}Al_5$ BMG possesses high macroscopic plasticity under compression at room temperature [11]. However, the contents of Al in the reported BMGs are relatively low, usually less than 15 at.% though in a few cases up to 25%. Further increasing the Al content often leads to a dramatic decrease in GFA in these alloys. Some unique properties are expected for Al-rich BMGs. Therefore, it is interesting to fabricate BMGs with high Al content, which are helpful for studying the effects of Al addition on GFA as well as the structure of BMG-forming alloys, and might provide clues for the eventual fabrication of Al-based BMGs. In this paper, we report the formation and properties of a class of BMGs with Al contents as high as 40%. The GFA, thermal properties as well as the mechanical properties of these alloys are studied. The effect of Al on the GFA is studied and discussed.

Al–RE (La, Ce, Gd, Y, Er)–Ni (Co) alloys with nominal compositions listed in Table 1 were prepared by arc melting mixtures of pure elements Al, La, Ce, Gd, Y, Er, Ni and Co in a Ti-gettered Ar atmosphere. The ingots were remelted and then poured into copper molds to obtain cylindrical rods. The amorphous nature was ascertained by X-ray diffraction (XRD) using a MAC Mo3 XHF diffractometer with Cu K_α radiation. Thermal analysis, comprising differential scanning calorimetry (DSC) and differential thermal analysis (DTA), was carried out in a Perkin Elmer DSC-7 and DTA-7, respectively. The mechanical behavior was tested under uniaxial compressive deformation mode at room temperature using an Instron 5500R1186 machine with a constant strain rate of $1 \times 10^{-4}\ s^{-1}$. ^{27}Al nuclear magnetic resonance (NMR) spectroscopy was performed at

* Corresponding author. E-mail: whw@aphy.iphy.ac.cn

1359-6462/$ - see front matter © 2008 Acta Materialia Inc. Published by Elsevier Ltd. All rights reserved.
doi:10.1016/j.scriptamat.2008.08.003

Table 1. Thermal parameters, fragility parameter and mechanical properties in Al-rich BMGs, and La-based BMGs with low Al content

Alloys	T_g (K)	T_x (K)	T_m (K)	T_l (K)	ΔT_m (K)	ΔT_x (K)	T_{rg}	γ	m	ε_f (%)	σ_f (MPa)	Isotropic Knight shift (ppm)
$Al_{40}La_{35}Y_{10}Ni_{15}$	586	627	909	1092	183	41	0.536	0.374	61	1.92	1309	595
$Al_{35}La_{33}Gd_{17}Ni_{10}Co_5$	560	609	748	1070	322	49	0.523	0.374	57	1.92	1050	–
$Al_{35}La_{30}Ce_{20}Ni_{15}$	542	577	822	1082	260	35	0.501	0.355	52	2.84	1158	–
$Al_{35}Gd_{33}Er_{17}Co_{15}$	586	620	1072	1221	149	34	0.524	0.362	70	2.19	817	–
$Al_{40}La_{45}Ni_{15}$	540	600	782	1097	315	60	0.492	0.367	59	1.97	1254	619
$Al_{35}La_{50}Ni_{15}$	532	596	784	971	187	64	0.548	0.397	44	1.86	1112	630
$Al_{25}La_{55}Cu_{10}Ni_5Co_5$ [12]	460	527	661	823	162	67	0.566	0.411	–	–	~860	–
$Al_{25}La_{55}Ni_{20}$ [13]	476	545	–	–	–	69	–	–	–	1.5	515	–
$Al_{14}La_{66}Cu_{10}Ni_{10}$ [13]	414	445	671	732	61	31	0.565	0.388	–	–	561	680

78.9729 MHz using a pulsed spectrometer. ^{27}Al Knight shifts are referenced to 1 M $Al(NO_3)_3$ aqueous solution.

Figure 1 shows XRD patterns of four as-cast BMGs with high Al contents, varying from 35% to 40%; only broad diffraction peaks can be seen within the resolution limit of the XRD for all the samples, indicating that amorphous rod can be obtained for alloys of at least 1 mm in diameter. We note that there could be small traces of crystalline phases in the sample. The $Al_{35}La_{50}Ni_{15}$ alloy can be cast into glassy rods at least 5 mm in diameter, suggesting the excellent GFA of these alloys. It is notable that in these alloys Al has become the most abundant single element, only slightly less than the combined contents of RE elements. For $Al_{40}La_{35}Y_{10}Ni_{15}$, the Al content reaches up to 40%, which is the highest Al content among the known BMGs reported so far. All the compositions of the Al-rich BMGs are listed in Table 1.

Figure 2 shows the DSC curve of typical $Al_{40}La_{35}Y_{10}Ni_{15}$ BMG, which exhibits a broad endothermic reaction due to glass transition, and one sharp exothermic peak due to crystallization. The inset of Figure 2 shows a DTA curve of the alloy exhibiting four exothermic signals due to melting. The melting temperature T_m and the liquidus temperature T_l are determined to be 909 and 1092 K, respectively: the difference between them ($\Delta T_m = T_l - T_m$) is 183 K, which is a high value. The multistage melting process and large ΔT_m indicate that

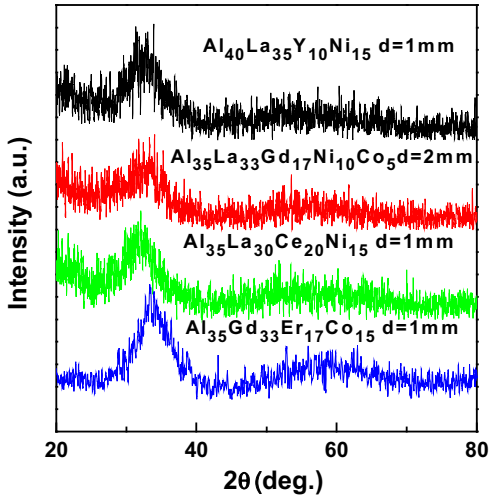

Figure 1. XRD patterns of four as-cast BMGs with high Al content.

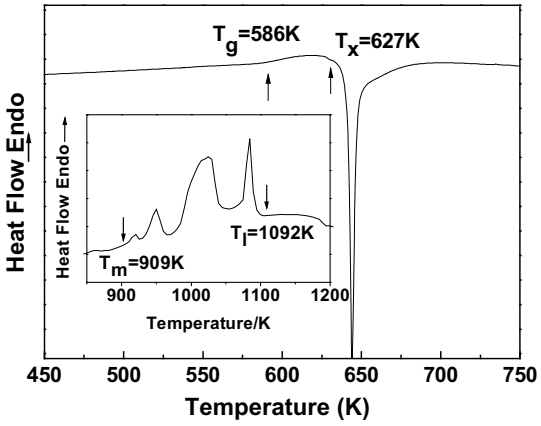

Figure 2. DSC and DTA (inset) curves of the as-cast $Al_{40}La_{35}Y_{10}Ni_{15}$ alloys. Scanning rate is 20 K min^{-1} for DSC and 10 K min^{-1} for DTA.

the alloy deviates greatly from the eutectic point. The glass transition temperature T_g and crystallization temperature T_x for $Al_{40}La_{35}Y_{10}Ni_{15}$ are determined to be 586 and 627 K, respectively, which are much higher than those of the Al–La–Y–Ni(Cu,Co) BMG with low Al content [12,13] as shown in Table 1, suggesting that this BMG has high thermal ability. The reduced glass transition temperature $T_{rg}(T_{rg} = T_g/T_l)$, the supercooled liquid region $\Delta T_x(\Delta T = T_x - T_g)$, and the γ value $[\gamma = T_x/(T_l + T_g)]$, which are effective parameters for evaluating the GFA of an alloy, are 0.536, 41 K and 0.374, respectively, which are relatively smaller than those of other reported BMGs [14]. The thermal parameters of the Al-rich BMGs are listed in Table 1. Generally, an alloy with good GFA is associated with $T_{rg} > 0.6$ [15,16], which often means the alloy is located at or near eutectic points. The present alloys, which are seriously off-eutectic with T_{rg} in the range 0.49–0.55, have unexpectedly good GFA. It is noticeable that Al-based metallic glassy ribbons are also off-eutectic with T_{rg}s of around 0.5, which are similar to that of our alloys. The above results imply that it is possible to obtain Al-rich BMGs with serious off-eutectic composition and low T_{rg} by proper selection of elements. The results may be helpful for investigating Al-based BMGs.

The fragility parameter m for $Al_{40}La_{35}Y_{10}Ni_{15}$, which is determined from the dynamic nature of the glass transition [17–19], is 61. The Vogel–Fulcher temperature T_o and the crystallization activation energy are determined

to be 572 K and 3.18 eV, respectively. The values of m for the Al-rich BMGs are in the range of 50–70 as listed in Table 1. These values can be classified as intermediate fragile liquids in the framework of fragility based on Angell's classification [17] and are larger than those of the other RE- ($m \sim 21$–32) [17,19], Zr- ($m \sim 34$–39) [20], Fe- ($m \sim 32$–37) [21] and Mg- ($m \sim 41$) based BMGs (all these values are evaluated using the same approach, which shows an obvious strong liquid behavior). The fragility provides a measure of the sensitivity of the structure of a liquid to temperature change, reflecting the dynamic behavior of supercooled liquids. In fragile liquids, the difference between the liquid and crystalline specific heats is relatively large, so that the Kauzmann temperature often falls not far below the temperature range where experiments can still detect relaxation phenomena. The Al-rich, fragile, glass-forming alloys showed good GFA and may therefore be useful candidates for investigating the glass transition.

Figure 3 shows the uniaxial compressive stress–strain curve of $Al_{40}La_{35}Y_{10}Ni_{15}$ alloy. After about ~1.9% elastic strain, the alloy fractured catastrophically, suggesting the brittle fracture behavior of this BMG, which is very similar to that of other BMGs [22]. However, the fracture strength for this alloy is as high as 1.31 GPa. Other Al-rich BMGs also have high fracture strength, all exceeding 1000 MPa except $Al_{35}Gd_{33}Er_{17}Co_{15}$alloy, and are hence much higher than those of the BMGs with low Al content as shown in Table 1. $Al_{35}La_{30}Ce_{20}Ni_{15}$ BMG even exhibits some limited plastic strain (~1%) after elastic strain.

The elastic moduli of BMGs correlate with T_g, T_m and mechanical properties and liquid fragility, and the elastic moduli of BMGs can be approximated by the weighted average of the elastic constants of their constituents due to the dense packing structure of BMGs and the metallic bond nature among the constituents [14]. Aluminum has been considered to possess some metalloid character when alloying with other metals [23], which can be seen from the high melting points of compounds in the Al-rich region of Al–RE or Al–TM binary phase diagrams [24] and the covalent character of Al–TM(Fe,Co) local bonds in some Al-rich amorphous alloys [25]. Thus, when the Al contents increased to solvent level in BMGs, a specific amorphous structure and novel properties are expected. Figure 4 shows the experimental and theoretical variation trends of T_g, T_x and fracture strength σ_f with Al content in Al–La–Ni(Cu,Co) BMGs. The theoretical values for T_g, T_x and σ_f are calculated based the correlations and elastic modulus rule in BMGs ($T_g \sim 2.5E$, $\sigma_f \sim E/50$ and $E^{-1} = \sum f_i E_i^{-1}$) [14]. It can be seen that the thermal stability (T_x), T_g and fracture strength (σ_f) of the Al-rich BMGs show a much larger increase than the calculated values with increasing Al content. This indicates that these Al-rich BMGs possess a unique amorphous structural and/or electronic structural evolution with change in Al concentration.

To probe the local structural and electronic structural evolution at Al sites and its implication for the general properties of the BMGs, ^{27}Al NMR was also measured systematically in $Al_x(La,Y)_{85-x}(Ni,Cu)_{15}$ ($x = 14$, 25, 35 and 40) BMGs. Figure 5a and b show the fracture strength as a function of Al concentration and ^{27}Al NMR Knight shift, respectively. Here, the fracture strength correlates better with the Knight shift than the Al concentration. As shown in Table 1, the Knight shifts are small compared to that of Al metal (1630 ppm). The shift decreases from ~680 to ~595 ppm as the concentration of Al increases from 14% to 40%. A similar observation was also reported by an earlier NMR study of the binary metallic glasses $La_{100-x}Al_x$ ($18 \leqslant x \leqslant 45$) [26]. The possible mechanism for the small Knight shift is the large reduction in the s character of the wave function at the Fermi level [27]. This could be attributed to the Al sp energy band splitting due to the lack of Al–Al nearest neighbors [28], leading to the Al 3s being localized far below the Fermi level, while Al 3p broadened across the Fermi level and hybridized with the matched d energy levels of surrounding elements around Al sites. This pd hybridization could lead to stronger directional bonding between Al and its nearest neighbors. The decrease in the Knight shift with increasing Al concentration and other composition changes favors the increase in the fracture strength in this alloy system (see Fig. 5b). This

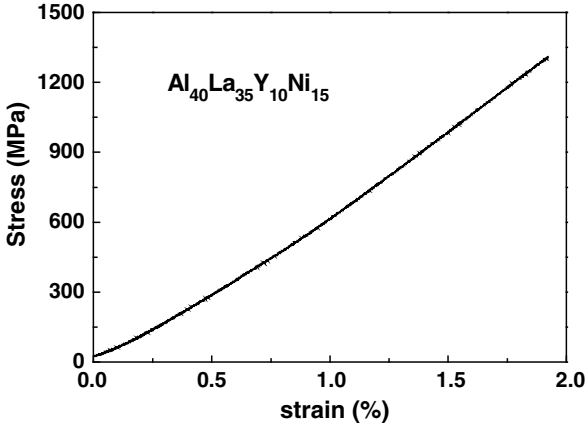

Figure 3. Engineering stress–strain curve of the as-cast $Al_{40}La_{35}Y_{10}Ni_{15}$ BMG with a strain rate of $1 \times 10^{-4}\,s^{-1}$ at room temperature.

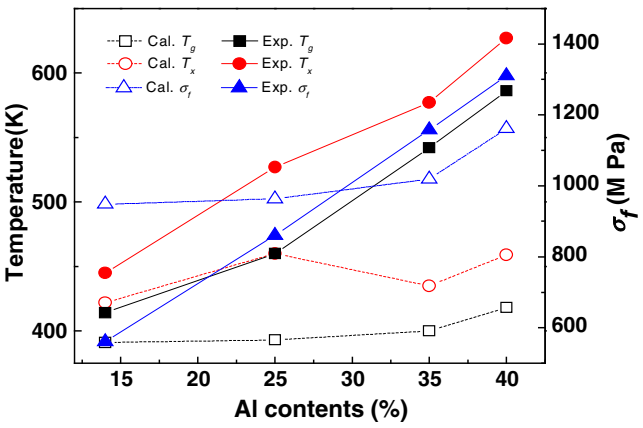

Figure 4. The experimental and theoretical variation of T_g, T_x with the Al contents in the Al-bearing BMGs. (The solid and dashed lines represent experimental and theoretical variations, respectively.)

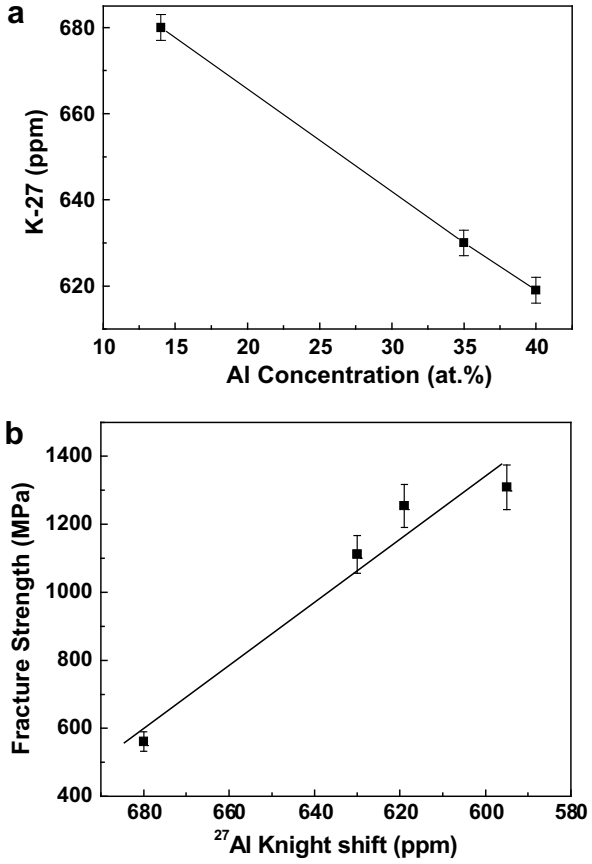

Figure 5. (a) ^{27}Al spectra of Al–La(Y)–Ni(Cu) BMGs at room temperature. The numbers in the figure are peak shifts (in ppm) referenced to 1 M $Al(NO_3)_3$. (b) Correlation of ^{27}Al Knight shifts with fracture strength of $Al_x(La,Y)_{85-x}(Ni,Cu)_{15}$ ($x = 14, 25, 35, 40$) BMGs at various Al concentrations. A straight line was drawn as a visual guide.

indicates that the ^{27}Al Knight shift is a useful measure of the electronic structure that determines some of the mechanical properties of Al-containing BMGs.

In summary, we report the formation and properties of a class of Al-rich BMGs with Al content as high as 40%. Compared to the reported BMGs with similar components but with low Al contents, these high Al-bearing BMGs deviate greatly from eutectic composition and show higher thermal stability, large values of fragility and considerably higher mechanical strength. These Al-rich BMGs can serve as a model system to study the role of Al in BMG formation and might have implications for investigating Al-based BMGs.

The authors are grateful to the financial support of the Natural Science Foundation of China (Nos. 50731008 and 50621061), CAS and MOST 973 (No. 2007CB613904).

[1] J. Schroers, W.L. Johnson, Phys. Rev. Lett. 93 (2004) 255506.
[2] W.H. Wang, Prog. Mater. Sci. 52 (2007) 540.
[3] A. Inoue, N. Nishiyama, MRS Bull. 32 (2007) 651.
[4] S. Li, W.H. Wang, Sci. Technol. Adv. Mater. 6 (2005) 823.
[5] X.J. Gu, J. Poon, Acta Mater. 56 (2008) 88;
Q.P. Cao, J.F. Li, Y. Zhou, Appl. Phys. Lett. 86 (2005) 081913.
[6] M.B. Tang, D.Q. Zhao, M.X. Pan, W.H. Wang, Chin. Phys. Lett. 21 (2004) 901.
[7] A.L. Greer, Science 267 (1995) 1947.
[8] Y. He, S.J. Poon, G.J. Shiflet, Science 241 (1988) 1640.
[9] F.Q. Guo, S.J. Poon, G.J. Shiflet, Mater. Sci. Forum 31 (2000) 331.
[10] A. Inoue, T. Zhang, W. Zhang, A. Takeuchi, Mater. Trans. JIM 37 (1996) 99.
[11] J. Das, M.B. Tang, K.B. Kim, R. Theissmann, F. Baier, W.H. Wang, J. Eckert, Phys. Rev. Lett. 94 (2005) 205501.
[12] A. Inoue, T. Nakamura, T. Sugita, T. Zhang, T. Masumoto, Mater. Trans. JIM 34 (1993) 351.
[13] M.L. Lee, Y. Li, C.A. Schuh, Acta Mater. 52 (2004) 4121.
[14] W.H. Wang, J. Appl. Phys. 99 (2006) 093506.
[15] W.L. Johnson, MRS Bull. 24 (1999) 42.
[16] D. Turnbull, Contemp. Phys. 10 (1969) 473.
[17] M.D. Ediger, C.A. Angell, S.R. Nagel, J. Phys. Chem. 100 (1996) 13200.
[18] L.N. Hu, X.F. Bian, W.M. Wang, J.Y. Zhang, Acta Mater. 52 (2004) 4773.
[19] Z.F. Zhao, Z. Zhang, W.H. Wang, Appl. Phys. Lett. 82 (2003) 4699;
B. Zhang, D.Q. Zhao, M.X. Pan, W.H. Wang, A.L. Greer, Phys. Rev. Lett. 94 (2005) 205502.
[20] D.N. Perera, J. Phys. Condens. Mater. 11 (1999) 3807.
[21] J.M. Borrego, A. Conde, S. Roth, J. Eckert, J. Appl. Phys. 92 (2002) 2073.
[22] S. Li, R.J. Wang, D.Q. Zhao, W.H. Wang, J. Non-Cryst. Solids 354 (2008) 1080.
[23] A. Inoue, A. Kitamura, T. Masumoto, J. Mater. Sci. 16 (1981) 1895.
[24] T.B. Massalski, Binary Alloy Phase Diagrams, second ed., ASM International, Materials Park, OH, 1990.
[25] A.N. Mansour, C.P. Wong, R.A. Brizzolara, Phys. Rev. B 50 (1994) 12401.
[26] D.P. Yang, W.A. Hines, C.L. Tsai, B.C. Giessen, F.C. Lu, J. Appl. Phys. 69 (1991) 6225.
[27] U. Mizutani, M. Tanaka, H. Sato, J. Phys. F Met. Phys. 17 (1987) 131.
[28] J. Hafner, S.S. Jaswal, Phys. Rev. B 38 (1988) 7320.